# research papers

# Structure-assisted discovery of *Variola major* H1 phosphatase inhibitors

**Jason Phan,‡ Joseph E. Tropea and David S. Waugh***

Macromolecular Crystallography Laboratory, Center for Cancer Research, National Cancer Institute at Frederick, PO Box B, Frederick, MD, USA

‡ Present address: Structural Biology Laboratory, Department of Drug Discovery, H. Lee Moffitt Cancer Center and Research Institute, Tampa, Florida, USA.

Correspondence e-mail: waughd@ncifcrf.gov

*Variola major* virus, the causative agent of smallpox, encodes the dual-specificity H1 phosphatase. Because this enzyme is essential for the production of mature virus particles, it is an attractive molecular target for the development of therapeutic countermeasures for this potential agent of bioterrorism. As a first step in this direction, the crystal structure of H1 phosphatase has been determined at a resolution of 1.8 Å. *In silico* screening methods have led to the identification of several small molecules that inhibit *Variola* H1 phosphatase with $IC_{50}$ values in the low micromolar range. These molecules provide novel leads for future drug development.

## 1. Introduction

Reversible protein phosphorylation, mediated by kinases and phosphatases, is a central mechanism of signal transduction in higher eukaryotes that regulates cell development, differentiation and death (Hunter, 1995). As such, the modulation of phosphorylation offers a potential means of therapy for a wide variety of maladies. Most protein kinases phosphorylate either tyrosine or serine and threonine residues (Taylor *et al.*, 1995). Protein phosphatases come in three common varieties: the protein tyrosine phosphatases (PTPases), the serine/threonine phosphatases and the dual-specificity phosphatases (DUSPs), which are capable of dephosphorylating tyrosine, serine and threonine residues (Martell *et al.*, 1998). Although the relatively large number of protein kinases (428) and phosphatases (99) encoded by the human genome (Ducruet *et al.*, 2005) naturally raises some concerns about the specificity of inhibitors, potent and specific inhibitors of both classes of enzymes have been developed in recent years, providing proof of principle for this method of therapeutic intervention (*e.g.* Sohn *et al.*, 2003; Sawyer *et al.*, 2005).

Certain viruses and bacterial pathogens of plants and animals also encode kinases and phosphatases that contribute to virulence by modulating host signal transduction pathways (Leader, 1993; Cozzone, 2005). Accordingly, these enzymes are considered to be attractive molecular targets for the development of therapeutic agents to combat the infectious diseases that they cause. For instance, the protein tyrosine phosphatase YopH has been the focus of efforts to develop countermeasures for *Yersinia pestis*, the causative agent of plague and a potential agent of bioterrorism (Lee *et al.*, 2003, 2005; Liang *et al.*, 2003; Phan *et al.*, 2003; Sun *et al.*, 2003; McCain *et al.*, 2004; Hu & Stebbins, 2005; Tautz *et al.*, 2005). Similarly, although officially eradicated (Stewart & Devlin,

2005), the smallpox virus (*Variola major*) is still considered to represent a potential bioterrorist threat (Harrison *et al.*, 2004). *Variola* virus encodes a dual-specificity protein phosphatase (H1) that is essential for viral replication (Liu *et al.*, 1995) and may therefore present an opportunity for therapeutic intervention. In addition to providing potential therapy for infected people, the availability of antiviral drugs could decrease the risks associated with the smallpox vaccine by providing an alternative for vaccine-sensitive individuals.

Common starting points for the development of enzyme inhibitors include substrate analogs, random screening and *in silico* screening (Bleicher *et al.*, 2003). Irrespective of which approach is taken, detailed information about the three-dimensional structure of the target enzyme and its complexes with inhibitors is highly desirable. Although the structures of several dual-specificity protein phosphatases have been determined (*e.g.* Yuvaniyama *et al.*, 1996; Fauman *et al.*, 1998; Farooq *et al.*, 2001, 2003; Kozlov *et al.*, 2004; Jeong *et al.*, 2005; Sun *et al.*, 2005; Yoon *et al.*, 2005; Jeong, Cho *et al.*, 2006; Jeong, Yoon *et al.*, 2006), none of them are similar enough to H1 phosphatase to enable an accurate homology model to be constructed. In order to overcome this difficulty, we successfully determined the structure of this crucial viral protein and employed an *in silico* screening strategy to identify several lead compounds with IC$_{50}$ values in the low micromolar range for further development.

## 2. Materials and methods

### 2.1. Crystallization, derivatization and data collection

Recombinant H1 phosphatase was overproduced and purified as described by Tropea *et al.* (2006), while the incorporation of selenomethionine followed the procedure of Doublié (1997). The peak fractions from a gel-filtration column corresponding to monomeric enzyme were pooled and concentrated to 8.5 mg ml$^{-1}$ in 50 m$M$ MES buffer pH 6.0. Sparse-matrix screens from Hampton Research were set up using a Hydra II Plus One (Matrix Technologies) crystallization robot and multiple hits were observed after a few days. At a 1:4 ratio of protein to precipitant, Hampton Research (HR) Index Screen condition No. 47 (28% polyethylene glycol monomethyl ether 2000, 0.1 $M$ bis-Tris pH 6.5) and HR PEG/Ion Screen condition No. 2 (20% polyethylene glycol 3350, 0.2 $M$ potassium fluoride) yielded thin trapezoid and rhombic plates that scattered X-rays, but not well enough for data collection. Therefore, HR Index Screen condition No. 47 was used in a PEG MME 2000 grid to scan for the optimal potassium fluoride concentration, leading to the identification of two crystal forms: *P*4 (24% PEG MME 2000, 1.7 $M$ KF, 0.1 $M$ bis-Tris pH 6.5) and *C*222$_1$ (20% PEG MME 2000, 0.6 $M$ KF, 0.1 $M$ bis-Tris pH 6.5). Additionally, attempts to cocrystallize H1 phosphatase with sodium orthovanadate, a competitive inhibitor of PTPases, yielded yet another type of tetragonal crystal (*I*4$_1$22) even though the ion did not bind. These conditions consisted of 26% PEG MME 2000, 1.5 $M$ KF,

**Table 1**
Crystallographic data, phasing and refinement statistics.

Values in parentheses are for the last shell.

| | | |
|---|---|---|
| Space group | $I4_122$ | |
| Unit-cell parameters (Å) | $a = b = 101.4, c = 95.1$ | |
| Data set | Se peak | Se inflection |
| Wavelength (Å) | 0.9792 | 0.9794 |
| Resolution (Å) | 25–1.8 (1.86–1.8) | 25–2.0 (2.07–2.0) |
| Unique reflections | 22420 | 16386 |
| Completeness (%) | 96.0 (97.8) | 95.2 (98.0) |
| Redundancy | 7.5 (7.2) | 7.6 (7.3) |
| $I/\sigma(I)$ | 12.9 (5.0) | 16.1 (4.4) |
| $R_{merge}$† (%) | 10.0 (39.0) | 8.6 (39.0) |
| No. of sites | 9 | |
| Phasing power | | |
|   Anomalous | 1.30 | |
|   Isomorphous (centric/acentric) | 0.42/0.49 | |
| Correlation coefficient (25–1.8 Å) | | |
|   After density modification | 0.92 | |
|   $R$ factor for $F_c$ *versus* $F_o$ | 0.14 | |
| Refinement resolution (Å) | 25–1.8 | |
| $R_{cryst}$ (%) | 17.8 | |
| $R_{free}$ (%) | 19.5 | |
| Ramachandran plot | | |
|   Most favorable (%) | 88.6 | |
|   Allowed (%) | 11.4 | |
| Average $B$ factor (Å$^2$) | 31.8 | |
| $B$ factor from Wilson plot (Å$^2$) | 28.9 | |
| R.m.s.d. bonds (Å) | 0.021 | |
| R.m.s.d. angles (°) | 1.62 | |
| No. of molecules in ASU | | |
|   Polypeptide | 1 | |
|   Solvent | 190 | |

† Friedel-related reflections were treated as equivalent.

3 m$M$ Na$_3$VO$_4$ and 0.1 $M$ bis-Tris pH 6.5 with a protein: precipitant ratio of 3:1.

Native data were collected for all three space groups to 2.0 Å with high completeness and the coordinates of human vaccinia H1-related phosphatase (PDB code 1vhr) were used as a search model in an attempt to solve the structure by molecular replacement. Since no credible solution was found, conventional heavy-atom compounds were screened using all crystal forms, but no useful derivative was obtained. Finally, the structure was solved by the multiwavelength anomalous dispersion (MAD) technique using selenomethionine-substituted protein. Fortuitously, the selenomethionyl protein crystallized reproducibly in the space group with the highest symmetry (*I*4$_1$22) under the same conditions as the native protein. The mother liquor was supplemented with 5% glycerol as a cryoprotectant before flash-freezing the crystals for data collection at SER-CAT insertion-device beamline 22-ID (Advanced Photon Source, Argonne National Laboratory). A fluorescence scan of the selenomethionine-derivative crystal confirmed the incorporation of Se atoms. Data were collected at the absorption edge and the peak wavelengths and were reduced using the *HKL*-2000 suite of programs (Otwinowski & Minor, 1997).

### 2.2. Structure determination and refinement

Highly redundant 1.8 Å MAD from the *I*4$_1$22 crystal were used in the *SHARP* program (de La Fortelle & Bricogne,

1997) to solve the structure. High-occupancy selenium positions were located for all but the N-terminal selenomethionine. After density modification, the correlation coefficient was 0.92 and the $R$ factor for $F_c$ versus $F_o$ was 0.14 for data in the resolution range 25–1.8 Å (Table 1). The structure was traced automatically using the program *ARP/wARP* (Morris *et al.*, 2004) as implemented in the *SHARP* interface. Manual correction of the model was carried out using the graphics software *O* (Jones *et al.*, 1991) and the SeMet-substituted structure was refined against the peak data using *REFMAC*5 (Murshudov *et al.*, 1997). Structure validation was accomplished using *PROCHECK* (Laskowski *et al.*, 1993).

### 2.3. Molecular modeling

The well refined model of *Variola* H1 phosphatase was loaded into *SYBYL* 7.0 (Tripos Inc.), where solvent molecules were removed, H atoms added and charges assigned. The structure was then used as the receptor for a virtual screen of the Diversity Set of 1990 compounds from the Developmental Therapeutics Program of the National Cancer Institute using the program *AutoDock* 3.05 (Morris *et al.*, 1998). The Olson group at the Scripps Research Institute have composed a virtual library of these compounds by adding H atoms and partial atomic charges and have made it available for use with *AutoDock*. The docking grid was centered on the S atom of the catalytic cysteine with a radius of 7.4 Å. The Lamarckian genetic algorithm was used at default settings for ligand conformational search. Top hits with inhibition constants in the micromolar range were re-scored with the program *X-score* for additional filtering of the active compounds (Wang *et al.*, 2002). Although the scoring function in *AutoDock* is known to be reasonably accurate, *X-score* uses a large training set based on real experimental data for macromolecular ligand-binding interactions.

### 2.4. Enzyme assays

The *Variola* H1 phosphatase-catalyzed reaction was conducted at room temperature using *p*-nitrophenol phosphate (pNPP) as the substrate in 1 ml of assay buffer containing 100 m*M* bis-Tris pH 6.5, 1 m*M* dithiothreitol, 1 m*M* ethylenediaminetetraacetic acid and 10% dimethylsulfoxide.

For inhibition assays, approximately 5 µg enzyme was pre-incubated with various concentrations of the inhibitor for 10 min before adding substrate to a final concentration of 200 µ*M* (approximately equal to the $K_M$) to initiate the reaction. The developing product was monitored continuously for 3 min at 405 nm on a Shimadzu UV–Vis spectrophotometer. The average absorbance per unit time was calculated using the installed kinetics program at various inhibitor concentrations and converted to the amount of product formed using a molar extinction coefficient of 18 000 $M^{-1}$ cm$^{-1}$ for pNPP. The relative activity was plotted against the inhibitor concentration using the program *SigmaPlot* to determine $IC_{50}$ values.

## 3. Results and discussion

### 3.1. Crystallization and structure solution

The *Variola* H1 PTPase, which is strongly inhibited by monovalent salts *in vitro* (Tropea *et al.*, 2006), responded to changes in ionic strength by crystallizing in different space groups. Increasing the potassium fluoride concentration caused the enzyme to shift from the orthorhombic space group $C222_1$ to the primitive tetragonal group $P4$ or, in the presence of sodium orthovanadate, to $I4_122$. Surprisingly, the latter crystal form did not have vanadate bound in the active site even though the concentration of the ligand in the mother liquor exceeded 1 m*M*. This may have been a consequence of the relatively low affinity of H1 phosphatase for vanadate (data not shown) and/or a chemical reaction with some component of the crystallization cocktail (a yellow tint was observed upon mixing).

The structure of H1 phosphatase was solved in space group $I4_122$ by the multiwavelength anomalous diffraction (MAD) technique using selenomethionine-substituted protein (Table 1). The MAD-phased experimental map calculated at a resolution of 1.8 Å was of excellent quality, allowing automatic tracing of all residues except the N-terminal serine (a non-native residue introduced during cloning) and the four C-terminal amino acids. The structure in space group $C222_1$ was subsequently solved by molecular replacement (data not shown). Apart from differences in a few disordered side chains
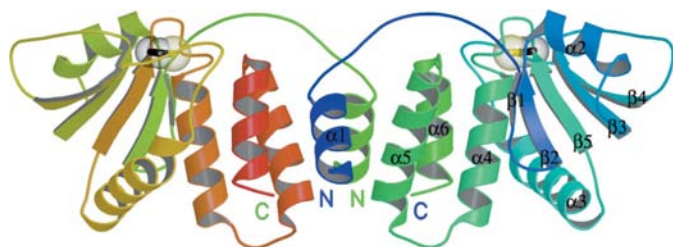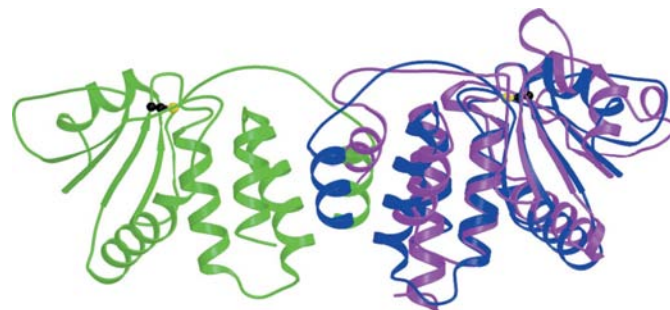


**Figure 1**
Ribbon model of the *V. major* H1 phosphatase shown with a rainbow coloring scheme. The enzyme crystallized as a domain-swapped dimer. The N- and C-termini of the two subunits are labeled in blue and green. The catalytic residue Cys110 is highlighted in bond and CPK format. Figs. 1 and 2 were prepared using the programs *MOLSCRIPT* (Kraulis, 1991) and *RASTER3D* (Merritt & Murphy, 1994).



**Figure 2**
Comparison of *Variola* H1 phosphatase with human VHR phosphatase. The ribbon model of the VHR monomer (magenta) is superimposed on a subunit of the H1 dimer (blue and green). The N-terminal helix of VHR has a similar conformation to that of the swapped molecule (green). The catalytic Cys110 of H1 is shown in ball-and-stick representation.

and loop regions, the $I4_122$ and $C222_1$ crystal forms yielded almost identical structures. The $C222_1$ structure was not refined because the virtually identical $I4_122$ structure was clearly of superior quality. The data obtained from the $P4$ crystals were not good enough to enable structure solution.

### 3.2. Description of the structure

In both crystal forms *Variola* H1 phosphatase crystallized as a domain-swapped dimer (Fig. 1), with the intermolecular axis lying along the crystallographic twofold axis. The swapped element is the N-terminal $\alpha$-helix, which rotates around a single bond in order to interact with the corresponding part of the neighboring molecule. As observed in other domain-swapped structures, the intermolecular interactions are mainly hydrophobic in nature (Nioche *et al.*, 2002). In the swapped position, the N-terminal helix forms a four-helix bundle with the three C-terminal helices from the adjacent molecule. It is oriented perpendicularly to the helix adjacent to the C-terminal helix and interacts with the corresponding element from the neighboring subunit at its base, while the two N-termini point away from each other at a right angle (Fig. 1). The N-terminal $\alpha$-helix could presumably adopt a very similar conformation to that of its swapped counterpart in an intramolecular configuration. The swapped helices are connected to the remainder of the polypeptides from which they originate by an 11-residue-long loop, giving *Variola* H1 phosphatase a distinctive appearance. It is unclear whether the observed dimer is biologically relevant or is just a crystallographic artifact (Tropea *et al.*, 2006). In any case, the environ-ment of the enzyme active site is not perturbed by the helix swapping.

### 3.3. Comparison with human vaccinia H1-related phosphatase (VHR) and other DUSPs

As expected, the overall fold of H1 phosphatase is similar to that of human vaccinia H1-related phosphatase (VHR; Fig. 2). A structural comparison with coordinates available from the Protein Data Bank using the program *DALI* (Holm & Sander, 1995) yielded five phosphatases with high alignment $Z$ scores: 18.0, 17.4, 13.9, 13.8 and 13.0 for human DUSP22 or JSP-1 (PDB code 1wrm), VHR (PDB code 1vhr), phosphoinositide phosphatase PTEN (PDB code 1d5r), cyclin-dependent kinase inhibitor 3 (PDB code 1fpz) and Cdc14b2 phosphatase (PDB code 1ohc), respectively. In such comparisons, $Z$ scores greater than 3.0 are usually considered to indicate significant structural similarity. However, all of these proteins have only limited sequence identity to H1 phosphatase, ranging from 13% to 28% for the aligned segments, which constitute 75–85% of their total lengths. Despite the high degree of structural similarity between H1 phosphatase, DUSP22 and VHR, the distribution of electrostatic potential and topographical details of the surfaces are quite different owing to the variation in their amino-acid sequences (Fig. 3). The negatively charged residues are concentrated at one end of the molecule (bottom) in VHR and, to a lesser extent, in DUSP22, whereas they are localized toward the middle in *Variola* H1. In the *Variola* H1 molecule, instead of negatively charged residues there is a long hydrophobic groove (bottom) left exposed by
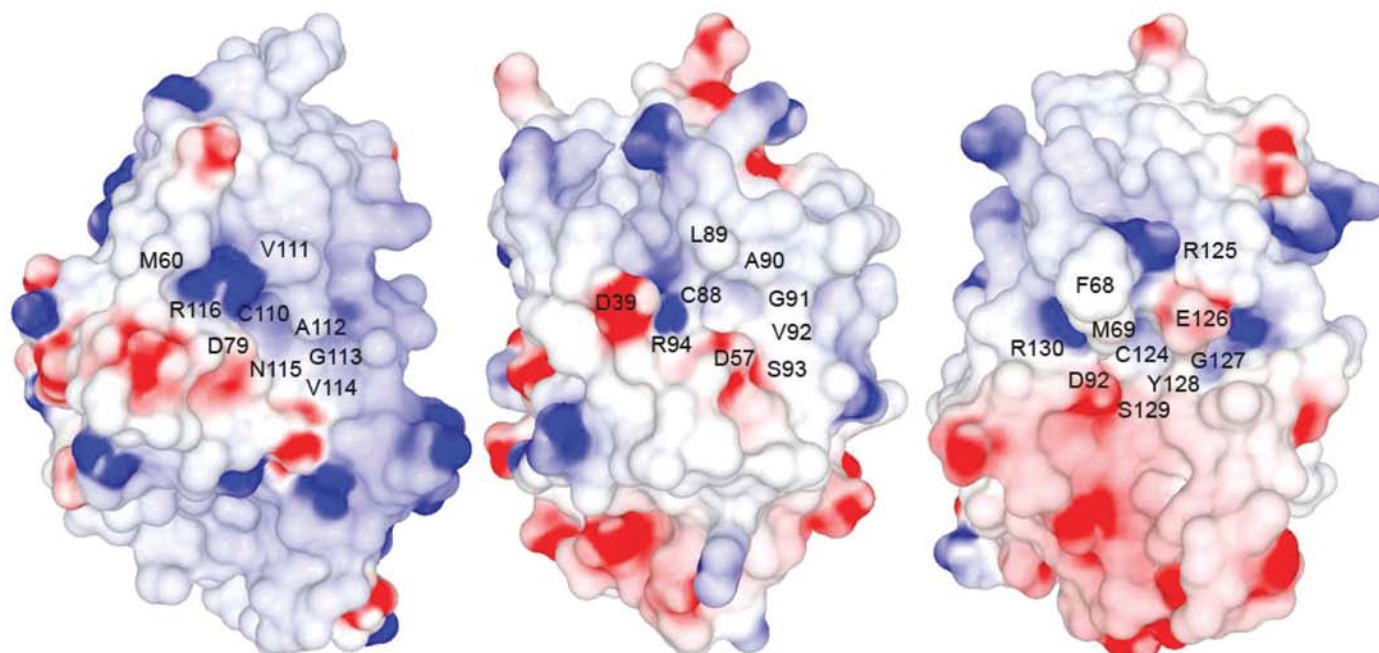


**Figure 3**
Space-filling models of the *Variola* H1 (left), human DUSP22 (center) and VHR (right) phosphatases with electrostatic potentials mapped onto their molecular surfaces. The potentials are colored from red ($-18kT/e$) to blue ($+18kT/e$), where $k$ is the Boltzmann constant, $T$ is the temperature and $e$ is the charge of the electron. White areas represent neutral and hydrophobic amino acids. The active-site residues, including the catalytic cysteine located at the bottom of the phosphate-binding loop, are labeled. This figure was prepared using *MOLSCRIPT* (Kraulis, 1991), *GRASP* (Nicholls, 1992) and *RASTER3D* (Merritt & Murphy, 1994).

the N-terminal helix that is involved in the intermolecular swapping interaction.

An alignment of multiple DUSP structures (Fig. 4) reveals a conserved core around the phosphate-binding loop comprised of the central β-sheet and the four C-terminal α-helices and several variable regions at both termini and the β3/β4, β4/α3 and α4/α5 loops (see Fig. 1 for numerical assignments of α-helices and β-strands). Additionally, there are two inserts that take the form of twisted loops between β2/α2 and β3/β4 that vary in length relative to the H1 phosphatase. The marked differences in the length and orientation of the N- and C-termini are a consequence of the fact that many of these DUSPs are multi-domain enzymes. Accordingly, rather than playing a role in substrate binding or catalysis, the sequences adjacent to the ends of these catalytic domains serve as linkers to other domains.

### 3.4. Analysis of the *Variola* H1 phosphatase active site

At the heart of all phosphatases is the highly conserved phosphate-binding loop comprised of the consensus sequence $HC(X)_5R(S/T)$, with the catalytic cysteine located in the center of the loop (Aqvist & Kolmodin, 2001; Denu & Dixon, 1998; Zhang, 1998). Superposition of the $C^\alpha$ traces of H1 and related phosphatases reveals that while the backbone amide groups of the loop residues ($X_5$) interact with the phosphate ion, their side chains determine the topology of the binding surface and therefore contribute to substrate specificity by lining the mouth of the active-site pocket. Furthermore, residues from the two insert loops β2/α2 and β3/β4 and the equivalent of the catalytic WPD loop in PTPases (loop β4/α3) shape the periphery of the substrate-binding pocket. More significantly, the aspartic acid Asp79 in the WPD-equivalent loop of H1 phosphatase (Asp57 and Asp92 in DUSP22 and VHR, respectively) occupies a similar position to the aspartic

acid residues in the classical PTPs (Asp356 in YopH; Asp181 in PTP1B; Asp425 in SHP-2; Asp1490 in LAR), which are known to act as the general acid during the enzyme-catalyzed hydrolysis of phosphotyrosine by these PTPases. The carboxylate groups of the WPD aspartates point toward the phenolic oxygen of the substrate phosphotyrosines. In the unbound H1 structure, the corresponding loop seems to be in the closed conformation, in which Asp79 instead interacts with the amide groups of Asn115 and Asn155.

The $X_5$ residues are very similar in H1 phosphatase and human DUSP22, but differ significantly from their equivalents in VHR and other enzymes (Fig. 3). They are Val, Ala, Gly, Val and Asn for H1, Leu, Ala, Gly, Val and Ser for DUSP22, and Arg, Glu, Gly, Tyr and Ser for VHR. The glycine in the $X_3$ position is invariant because it accommodates a necessary steric constraint on the phosphate-binding loops. The large and charged/polar side chains at positions $X_1$, $X_2$ and $X_4$ in VHR create a deeper and electrostatically different binding pocket compared with those of H1 and DUSP22. In addition, the side chain of Met69 in VHR is in hydrophobic contact with a methylene group of the bound HEPES molecule [4-(2-hydroxyethyl)-1-piperazineethanesulfonic acid], while the rest of the piperazineethane moiety stacks against the aliphatic part of Glu126 and the aromatic ring of Tyr128. In the PTEN structure, the side chain of Val45 lines the mouth of the active site, while the phenyl ring of Tyr46 packs against the aliphatic part of Lys125, a phosphate-binding loop residue. None of these interactions are possible in the H1 binding site because it lacks the insert loops and possesses Ala112 and Val114 instead of the longer side chains found in VHR and PTEN. Nevertheless, the side chains of Ala112, Val114 and Val111 effectively mimic the aliphatic portions of Glu126, Tyr128 and Arg125 in VHR or Ala126, Lys128 and Lys125 in PTEN, respectively, because the charged ends of these side chains in the latter two enzymes point away from the active site in a manner that maximally exposes their hydrophobic trunks. In effect, the active site of H1 phosphatase is broader and shallower than the active sites of the other DUSPs, with the exception of human DUSP22, which has almost identical amino acids in these positions. The only two $X_5$-loop residues that differ between H1 and DUSP22 are Val111 and Asn115, and Leu89 and Ser93 ($X_1$ and $X_5$), respectively. The serine in DUSP22 forms a hydrogen bond to the carboxylate group of the catalytic aspartate Asp57 (Asp79 and Asp92 in H1 and VHR, respectively) as opposed to the asparagine amide group, which makes a stronger hydrogen-bond donor. Furthermore, this amide group can also form a hydrogen bond with the phenolic oxygen of pTyr more readily than can the serine side chain. Otherwise, the two active sites are very similar in shape and size compared with those of other DUSPs, including human
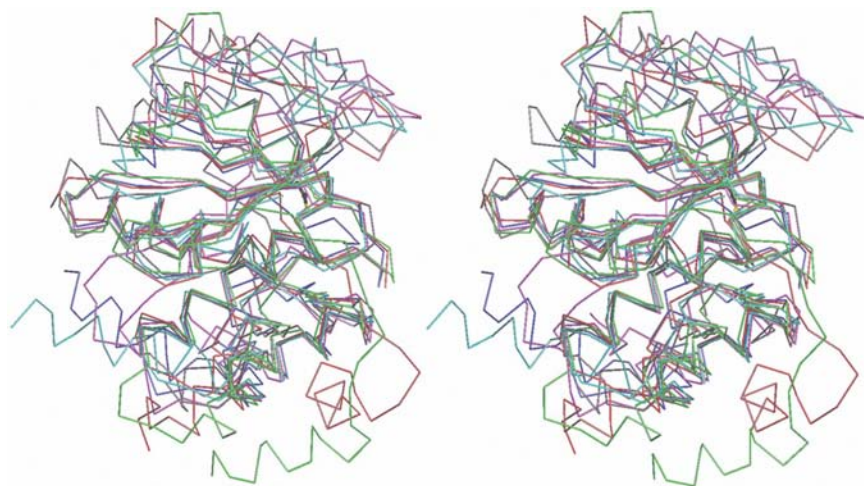


**Figure 4**
Superposition of the $C^\alpha$ traces of the six structurally similar DUSPs *Variola* H1 (green), human DUSP22 (blue), human VHR (red), phosphoinositide phosphatase PTEN (grey), cyclin-dependent kinase inhibitor 3 (magenta) and Cdc14b2 phosphatase (cyan) shown in stereoview. This figure was prepared using the program *O* (Jones *et al.*, 1991). See Fig. 1 for the numbering of α-helices and β-strands.

VHR. Therefore, DUSP22 appears to be the best enzyme with which to gauge the specificity of H1 phosphatase inhibitors.

## 3.5. Lead discovery

In an attempt to identify potential inhibitors, we used the high-resolution structure of H1 phosphatase as a starting point for *in silico* screening of the Structural Diversity Set of Compounds from the Developmental Therapeutics Program of the National Cancer Institute (Fig. 5). Of approximately two dozen top-scoring compounds that were tested, one third were found to be insoluble in aqueous solution. Four of the soluble compounds exhibited measurable inhibitory activity. These were NSC-62914, NSC-28086, NSC-105687 and NSC-23173, with $IC_{50}$ values of 48, 51, 212 and 342 μ*M*, respectively. *In silico* screening of the CalBiochem phosphatase-inhibitor library identified two additional compounds (catalog Nos. 540211 and 217691) as possible leads and these were subsequently shown to have $IC_{50}$ values against H1 phosphatase of 4 and 11 μ*M*, respectively.

All of the inhibitors identified above possess an aromatic ring adjacent to a polar head group, which is reminiscent of phosphotyrosine. Accordingly, this may indicate that the enzyme preferentially dephosphorylates phosphotyrosine residues rather than serine or threonine. The polar head groups of the inhibitors may interact with the phosphate-binding loop of the enzyme while the aromatic moiety stacks against the active-site arginine. Ligands with additional hydrophobic groups could potentially be accommodated by the shallow groove formed by alanine and valine residues at the mouth of the active site in H1 phosphatase. Developing inhibitors of H1 phosphatase and other DUSPs with high potency may present a significant challenge because of their comparatively shallow substrate-binding grooves. However, the prospects for developing inhibitors with high selectivity for H1 phosphatase seem promising because the substrate-binding sites of the dual specificity phosphatases exhibit a much greater degree of variability than do those of their PTPase counterparts.

A potential advantage of the H1 phosphatase inhibitors identified in this study is that they have been pre-filtered for favorable drug-like properties. Efforts to cocrystallize these inhibitors with the *Variola* enzyme are currently under way. It is hoped that the resulting structural information will reveal a common pharmocophore and suggest ways in which the potency and specificity of the inhibitors can be further improved. It will also be important to obtain at an early stage information about the specificity, toxicity and bioavailability of these compounds and their derivatives and appropriate resources are currently being assembled to address these issues. Although we hope that one will never be needed, the availability of an effective therapeutic countermeasure for the smallpox virus would be very reassuring indeed.
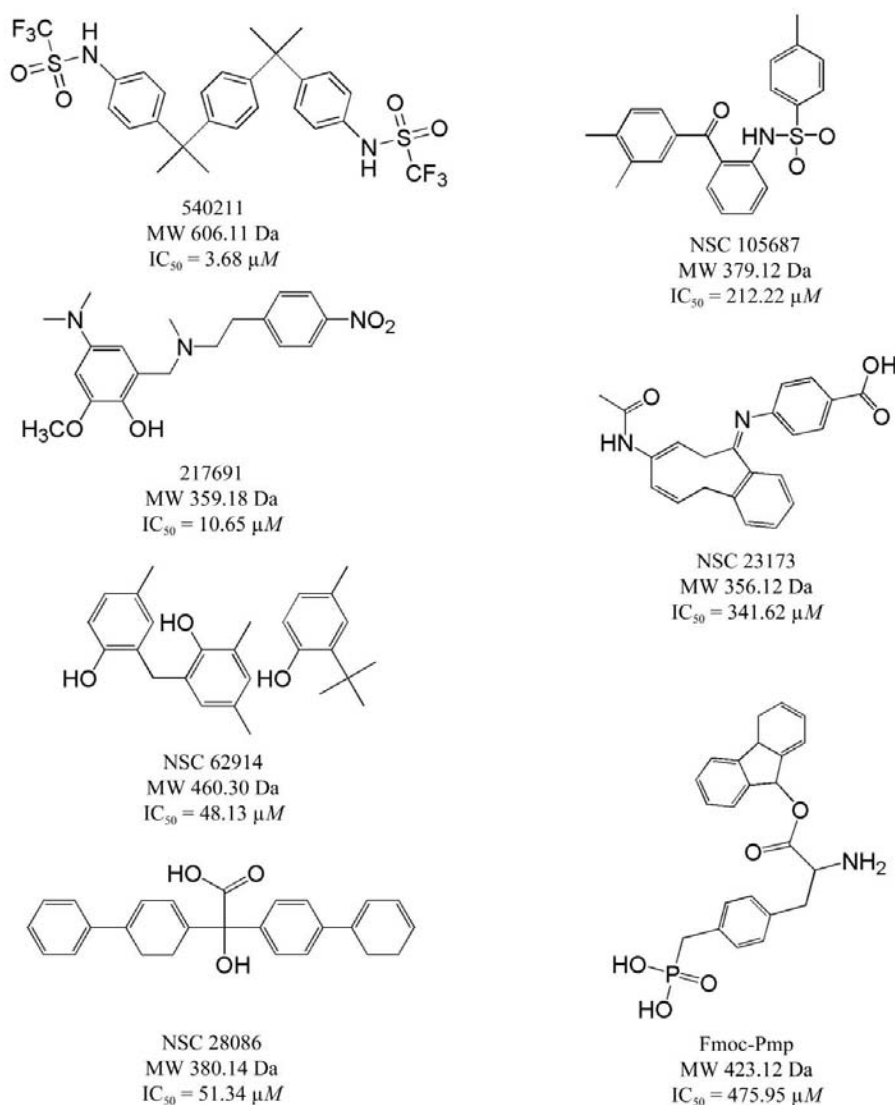
**Figure 5**
Structures, molecular weights and experimentally determined $IC_{50}$ values of the most potent inhibitors identified by virtual screening of *Variola* H1 phosphatase. This figure was prepared using *ChemDraw* (CambridgeSoft).

## References

Aqvist, J. & Kolmodin, K. (2001). *FEBS Lett.* **498**, 208–213.

Bleicher, K. H., Bohm, H. J., Muller, K. & Alanine, A. I. (2003). *Nature Rev. Drug Discov.* **2**, 369–378.

Cozzone, A. J. (2005). *J. Mol. Microbiol. Biotechnol.* **9**, 198–213.

Denu, J. M. & Dixon, J. E. (1998). *Curr. Opin. Chem. Biol.* **2**, 633–641.

Doublié, S. (1997). *Methods Enzymol.* **276**, 523–530.

Ducruet, A. P., Vogt, A., Wipf, P. & Lazo, J. S. (2005). *Annu. Rev. Pharmacol. Toxicol.* **45**, 725–750.

Farooq, A., Chaturvedi, G., Mujtaba, S., Plotnikova, O., Zeng, L., Dhalluin, C., Ashton, R. & Zhou, M.-M. (2001). *Mol. Cell*, **7**, 387–399.

Farooq, A., Plotnikova, O., Chaturvedi, G., Yan, S., Zeng, L., Zhang, Q. & Zhou, M.-M. (2003). *Structure*, **11**, 155–164.

Fauman, E. B., Cogswell, J. P., Lovejoy, B., Rocque, W. J., Holmes, W., Montana, V. G., Piwnica-Worms, H., Rink, M. J. & Saper, M. A. (1998). *Cell*, **93**, 617–625.

Harrison, S. C., Alberts, B., Ehrenfeld, E., Enquist, L., Fineberg, H., McKnight, S. L., Moss, B., O'Donnell, M., Ploegh, H., Schmid, S. L., Walter, K. P. & Theriot, J. (2004). *Proc. Natl Acad. Sci. USA*, **101**, 11178–11192.

Holm, L. & Sander, C. (1995). *Trends Biochem. Sci.* **20**, 478–480.

Hu, X. & Stebbins, C. E. (2005). *Bioorg. Med. Chem.* **13**, 1101–1109.

Hunter, T. (1995). *Cell*, **80**, 225–236.

Jeong, D. G., Cho, Y. H., Yoon, T. S., Kim, J. H., Son, J. H., Ryu, S. E. & Kim, S. J. (2006). *Acta Cryst.* D**62**, 582–588.

Jeong, D. G., Kim, S. J., Kim, J. H., Son, J. H., Park, M. R., Lim, S. M., Yoon, T. S. & Ryu, S. E. (2005). *J. Mol. Biol.* **345**, 401–413.

Jeong, D. G., Yoon, T. S., Kim, J. H., Shim, M. Y., Jeong, S. K., Son, J. H., Ryu, S. E. & Kim, S. J. (2006). *J. Mol. Biol.* **360**, 946–955.

Jones, T. A., Zou, J.-Y., Cowan, S. W. & Kjeldgaard, M. (1991). *Acta Cryst.* A**47**, 110–119.

Kozlov, G., Cheng, J., Ziomek, E., Banville, D., Ghering, K. & Ekiel, I. (2004). *J. Biol. Chem.* **279**, 11882–11889.

Kraulis, P. J. (1991). *J. Appl. Cryst.* **24**, 946–950.

de La Fortelle, E. & Bricogne, G. (1997). *Methods Enzymol.* **276**, 472–494.

Laskowski, R. A., MacArthur, M. W., Moss, D. S. & Thornton, J. M. (1993). *J. Appl. Cryst.* **26**, 283–291.

Leader, D. P. (1993). *Pharmacol. Ther.* **59**, 343–389.

Lee, K., Boovanahalli, S. K., Nam, K. Y., Kang, S. U., Lee, M., Phan, J., Wu, I., Waugh, D. S., Zhang, Z.-Y., No, K. T., Lee, J. J. & Burke, T. R. Jr (2005). *Bioorg. Med. Chem. Lett.* **15**, 4037–4042.

Lee, K., Gao, Y., Yao, Z. J., Phan, J., Wu, I., Liang, J., Waugh, D. S., Zhang, Z.-Y. & Burke, T. R. Jr (2003). *Bioorg. Med. Chem.* **13**, 2577–2581.

Liang, F., Huang, Z., Lee, S. Y., Liang, J., Ivanov, M. I., Alonso, A., Bliska, J. B., Lawrence, D. S., Mustelin, T. & Zhang, Z.-Y. (2003). *J. Biol. Chem.* **278**, 41734–41741.

Liu, K., Lemon, B. & Traktman, P. (1995). *J. Virol.* **69**, 7823–7834.

McCain, D. F., Wu, L., Nickel, P., Kassack, M. U., Kreimeyer, A., Gagliardi, A., Collins, D. C. & Zhang, Z.-Y. (2004). *J. Biol. Chem.* **279**, 14713–14725.

Martell, K. J., Angelotti, T. & Ullrich, A. (1998). *Mol. Cell*, **8**, 2–11.

Merritt, E. A. & Murphy, M. E. P. (1994). *Acta Cryst.* D**50**, 869–873.

Morris, G. M., Goodsell, D. S., Halliday, R. S., Huey, R., Hart, W. E., Belew, R. K. & Olson, A. J. (1998). *J. Comput. Chem.* **19**, 1639–1662.

Morris, R. J., Zwart, P. H., Cohen, S., Fernandez, F. J., Kakaris, M., Kirillova, O., Vonrhein, C., Perrakis, A. & Lamzin, V. S. (2004). *J. Synchrotron Rad.* **11**, 56–59.

Murshudov, G. N., Vagin, A. A. & Dodson, E. J. (1997). *Acta Cryst.* D**53**, 240–255.

Nicholls, A. (1992). *GRASP. Graphical Representation and Analysis of Surface Properties.* Department of Biochemistry and Molecular Biophysics, Columbia University, New York, NY, USA.

Nioche, P., Liu, W. Q., Broutin, I., Charbonnier, F., Latreille, M. T., Vidal, M., Roques, B., Garbay, C. & Ducruix, A. (2002). *J. Mol. Biol.* **315**, 1167–77.

Otwinowski, Z. & Minor, W. (1997). *Methods Enzymol.* **276**, 307–326.

Phan, J., Lee K., Cherry, S., Tropea, J. E., Burke, T. R. Jr & Waugh, D. S. (2003). *Biochemistry*, **42**, 13113–13121.

Sawyer, T. K., Shakespeare, W. C., Wang, Y., Sundaramoorthi, R., Huang, W. S., Metcalf, C. A. III, Thomas, M., Lawrence, B. M., Rozamus, L., Noehre, J., Zhu, X., Narula, S., Bohacek, R. S., Weigele, M. & Dalgarno, D. C. (2005). *Med. Chem.* **1**, 293–319.

Sohn, J., Kiburz, B., Li, Z., Deng, L., Safi, A., Pirrung, M. C. & Rudolph, J. (2003). *J. Med. Chem.* **46**, 2580–2588.

Stewart, A. J. & Devlin, P. M. (2005). *J. Infect.* **52**, 329–334.

Sun, J. P., Wang, W. O., Yang, H., Liu, S., Liang, F., Fedorov, A. A., Almo, S. C. & Zhang, Z.-Y. (2005). *Biochemistry*, **44**, 12009–12021.

Sun, J. P., Wu, L., Federov, A. A., Almo, S. C. & Zhang, Z.-Y. (2003). *J. Biol. Chem.* **278**, 33392–33399.

Tautz, L., Bruckner, S., Sareth, S., Alonso, A., Bogetz, J., Bottini, N., Pellecchia, M. & Mustelin, T. (2005). *J. Biol. Chem.* **280**, 9400–9408.

Taylor, S. S., Radzio-Andzelm, E. & Hunter, T. (1995). *FASEB J.* **9**, 1255–1266.

Tropea, J. E., Phan, J. & Waugh, D. S. (2006). *Protein Expr. Purif.* **50**, 31–36.

Wang, R., Lai, L. & Wang, S. (2002). *J. Comput. Aided Mol. Des.* **16**, 11–26.

Yoon, T. S., Jeong, D. G., Kim, J. H., Cho, Y. H., Son, J. H., Lee, J. W., Ryu, S. E. & Kim, S. J. (2005). *Proteins*, **61**, 694–697.

Yuvaniyama, J., Denu, J. M., Dixon, J. E. & Saper, M. A. (1996). *Science*, **272**, 1328–1331.

Zhang, Z.-Y. (1998). *Crit. Rev. Biochem. Mol. Biol.* **33**, 1–52.